Supplemental material: The hybrid approach - Convolutional Neural Networks and Expectation Maximization Algorithm - for Tomographic Reconstruction of Hyperspectral Images

Mads Juul Ahlebæk,[a] Mads Svanborg Peters,[b,c] Wei-Chih Huang,[a] Mads Toudal Frandsen[a], René Lynge Eriksen[c] and Bjarke Jørgensen[b]

[a]CP[3]-Origins, Department of Physics, Chemistry and Pharmacy, University of Southern Denmark, Denmark

[b]Newtec Engineering A/S, 5230 Odense, Denmark

[c]Mads Clausen Institute, University of Southern Denmark, Denmark

Contact

M.J. Ahlebæk: ahle@sdu.dk
https://orcid.org/0000-0003-4938-4802

M.T. Frandsen: frandsen@cp3.sdu.dk
https://orcid.org/0000-0003-2061-562X

M.S. Peters: mape@newtec.dk
https://orcid.org/0000-0002-5761-4586

R.L. Eriksen: rle@mci.sdu.dk
https://orcid.org/0000-0003-4405-5831

W.-C. Huang: wchi@newtec.dk
https://orcid.org/0000-0001-7939-3246

B. Jørgensen: bjarke@newtec.dk
https://orcid.org/0000-0001-8559-9435

S1 Introduction

This supplemental material accompanies the main paper and details the computed tomography imaging spectrometer (CTIS) simulator as well as the measurement of the parameters used in the simulator. Additionally, RGB visualizations of all the hyperspectral images capture with our VIS-NIR laboratory pushbroom system are shown. A selection of the reconstructed hyperspectral images for both the 25- and 100-channel cases are also compared through RGB visualizations.

S2 Computed Tomography imaging spectrometer simulator

The CTIS simulator introduced in our work is an updated version of the simulator used in our previous work[1], and is used to create input CTIS images for our networks. This updated simulator includes zero mean white Gaussian noise, a point-spread-function (PSF) and spectral sensitivity corrections due to the illuminant and the diffractive optic element (DOE). Thus, the simulator requires the following inputs; x, y, z, $b1$, $b2$, $shift$, $allOrders$, $diff\_sens$, $illum$, $sigma\_psf$, and $noise$. The first seven inputs determine the geometry of the simulated CTIS image while the latter three inputs determine the optical parameters.

Figure S1a shows an overview of how the geometric inputs correlate to the simulated CTIS image: x, y and z denote the two spatial and one spectral dimensions of the input respectively, i.e. the zeroth order size is defined by $x \times y$ and z denotes the number of spectral channels. $b1$ and $b2$ determine the number of pixels between the zeroth- and first orders and the first orders and the outer border of the image, respectively. $b2$ is usually set to zero, but is provided for generalizability. The $shift$ input determines the pixel shift between consecutive spectral channels in the first order diffraction spots. It should be mentioned that the user is responsible for setting the inputs to the correct values to match the true CTIS system, i.e. $b1$, $b2$ and $shift$ are not calculated in the simulator based on the wavelength of the spectral channels. The $allOrders$ input is a boolean parameter, which simulates all eight surrounding first order diffraction spots if set to 'True' and only the four (no skew orders) first order diffraction spots if set to 'False'.

The optical parameters of the CTIS system are defined by the $diff\_sens$, the $illum$ and the applied $noise$. Additionally, the point-spread-function (PSF), $sigma\_psf$, is set within the simulator, but is not available to the user as an input. The measurement of the PSF for the true CTIS system is detailed in Section S3. The $diff\_sens$ describes the wavelength- and diffraction order dependent sensitivity

and must be a matrix of dimensions $\#orders \times z$, i.e. in case of $allOrders = True$, $9 \times z$. The acquisition of the diffraction sensitivity is described in Section S4. The illuminant used in the simulator is a standard halogen-tungsten lamp, which is used for the acquisition of true CTIS images. The illumination input is a vector of size $1 \times z$, which contains the spectrum of the illuminant measure with an intensity calibrated Avaspec 2048x14 spectrometer operating in the 200-720nm range. The spectrometer was calibrated using a radiometrically calibrated light source (HL-3P-CAL) from Ocean Insights.

Figure S1b shows a simulated 450×450 pixels CTIS images of a $100 \times 100 \times 25$ white cube, i.e. all voxels are set to 1, with $b1 = 27$, $b2 = 0$, $shift = 2$, $allOrders = True$, $sigma\_psf = \sigma = 1.04$ pixels and $noise = 0.44$. The diffraction sensitivity and illumination is set to the values defined in Section S4.

S3 Measurements of the point spread function

The PSF of the CTIS system is determined using the slanted-edge method[2], where a sharp, slanted image is imaged and the PSF is estimated from the transition of the edge. In practice, a back illuminated razorblade is imaged by the CTIS camera (Figure S2a), and the edge-spread-function (ESF) (Figure S2c) is calculated as the mean profile across 250 pixels (blue rectangle) over the transition in the zeroth order (Figure S2b). The line-spread-function (LSF) is depicted in Figure S2d, and it is calculated as the derivative of the ESF, which is equivalent to a 2D slice of the PSF. Thus, assuming a spatially symmetric PSF, the LSF is an approximate estimate of the PSF. The standard deviation of the LSF (and PSF) is determined to be 1.04 pixels based on a Gaussian fit with $R^2 = 0.98$. The effect of the PSF on a single pixel is visualized in Figure S2e for a standard deviation of 1.04, which is the value used in the simulator.

S4 Measurement of diffraction sensitivity

The diffraction sensitivity of the CTIS system is measured using a monochromator (Newport mini, model: 78027) equipped with a halogen lamp (Tungsten Halogen Light Source, Model: 78043), which is calibrated with an intensity calibrated Avaspec 2048x14 spectrometer. The spectrometer is calibrated using a radiometrically calibrated light source (HL-3P-CAL) from Ocean Insights. Since the measurements are conducted with the whole CTIS system, both the diffraction efficiency of the DOE, the transmission of the optical system, the CMON image sensor response and optical aberrations are intrinsically a part of the acquire images. Thus, the measured diffraction sensitivity estimates the combination of all these contributions. The monochromator output is centered in the zeroth order of the CTIS image, and CTIS images and corresponding dark-frame images are captured for wavelengths ranging from 400-750 nm with 25 nm steps. For each wavelength, the exposure time of the CTIS is set to maximize the dynamic range of the image sensor, and the dark frame is captured at the same exposure. Figure S3a shows the superimposed CTIS images of the monochromator for 400-750 nm. To determine the diffraction sensitivity $S(\lambda, s)$ from the acquired images, the dark-frame is subtracted from the CTIS image, and the total photon count $PC(\lambda, s)$ for each diffraction spot (zeroth- and surrounding first orders) is divided with the product of the exposure time $t(\lambda)$ in μs, the camera gain $G(\lambda)$ (set to 1 for all images) and the wavelength correction factors $C(\lambda)$ from the spectrometer:

$$S(\lambda, s) = \frac{PC(\lambda, s)}{t(\lambda) \cdot G(\lambda) \cdot C(\lambda)} \tag{1}$$

Where λ and s denote the wavelength in nm and s the diffraction spot, respectively. The monochromator output (Figure S3b) is used to determine the correction factors $C(\lambda)$, which indicate the relative intensity of the monochromator output (area in blue under the curve). The total photon count of the respective diffraction spots $PC(\lambda, s)$ is determined from the acquired CITS images as the

total volume of each spot. Figure S3c shows the calculated diffraction sensitivity $S(\lambda, s)$, where the indices (i, j) of the diffraction spots indicate (rows, columns). The DOE is designed to achieve a symmetric diffraction efficiency in the first orders while minimizing the zeroth order. The diffraction sensitivity of the zeroth order $(0,0)$ is smallest for the lower wavelengths before increasing towards 700 nm, while the first order diffraction sensitivities all follow the same parabolic shape. However, the right-diagonal first orders $\{(-1,1)$ and $(1,1)\}$ have significantly lower diffraction sensitivity across the entire wavelength range. It should be noted, that since $S(\lambda, s)$ is only measured for 15 different wavelengths from 400-750 nm, the sensitivities are interpolated for the 25 and 100 channels used in this work.

S5 Measurement of halogen lamp illumination

The intensity calibrated Avaspec 2048x14 spectrometer is used to measure the output of an industrial halogen lamp used as illumination for the acquisition of CTIS images. Figure S4 shows the measured spectrum of the halogen lamp and a fitted black body with temperature of $T = 2952\ K°$, which is consistent with standard $T = 3000\ K°$ halogen lamps.

S6 RGB reconstruction of pushbroom hyperspectral cubes

Figures S5-S8 shows RGB reconstructions of the 178 hyperspectral images captured with the VIS-NIR pushbroom system, which were used to generate data sets of CTIS images for the networks. The RGB images are generated by combining three spectral channels at 470 nm (blue), 549 nm (green) and 650 nm (red).

S7 Comparison of RGB reconstructions for reconstructed hyperspectral cubes - 25 channels

Figures S9-S11 show comparisons of the ground truth (GT) RGB visualization with the reconstructed RGB images for EM (20 iterations), CNN, CNN-EM (10 iterations), EM (10 iterations)-CNN, UNet and UNet-EM (10 iterations) for various hyperspectral images. The RGB images are generated by combining the 7^{th}, 9^{th} and 13^{th} channel. Figure S9 and S10 contain seen cubes used in the training, while Figure S11 contains unseen cubes.

S8 Comparison of RGB reconstructions for reconstructed hyperspectral cubes - 100 channels

Figures S12-S14 show comparisons of the ground truth (GT) RGB visualization with the reconstructed RGB images for EM (20 iterations), CNN, CNN-EM (10 iterations), EM (10 iterations)-CNN, UNet and UNet-EM (10 iterations) for various hyperspectral images. The RGB images are generated by combining the 14^{th}, 29^{th} and 48^{th} channel. Figure S12 and S13 contain seen cubes used in the training, while Figure S14 contains unseen cubes.

References

1. W. -C. Huang, M. S. Peters, M. J. Ahlebæk, M. T. Frandsen, R. L. Eriksen and B. Jørgensen, Displays , 102218 (2022)
2. M. Estribeau and P. Magnan, in Detectors and Associated Signal Processing, Vol. 5251, edited by J.-P. Chatard and P. N. J. Dennis (SPIE, 2004) pp. 243 - 252, backup Publisher: International Society for Optics and Photonics.

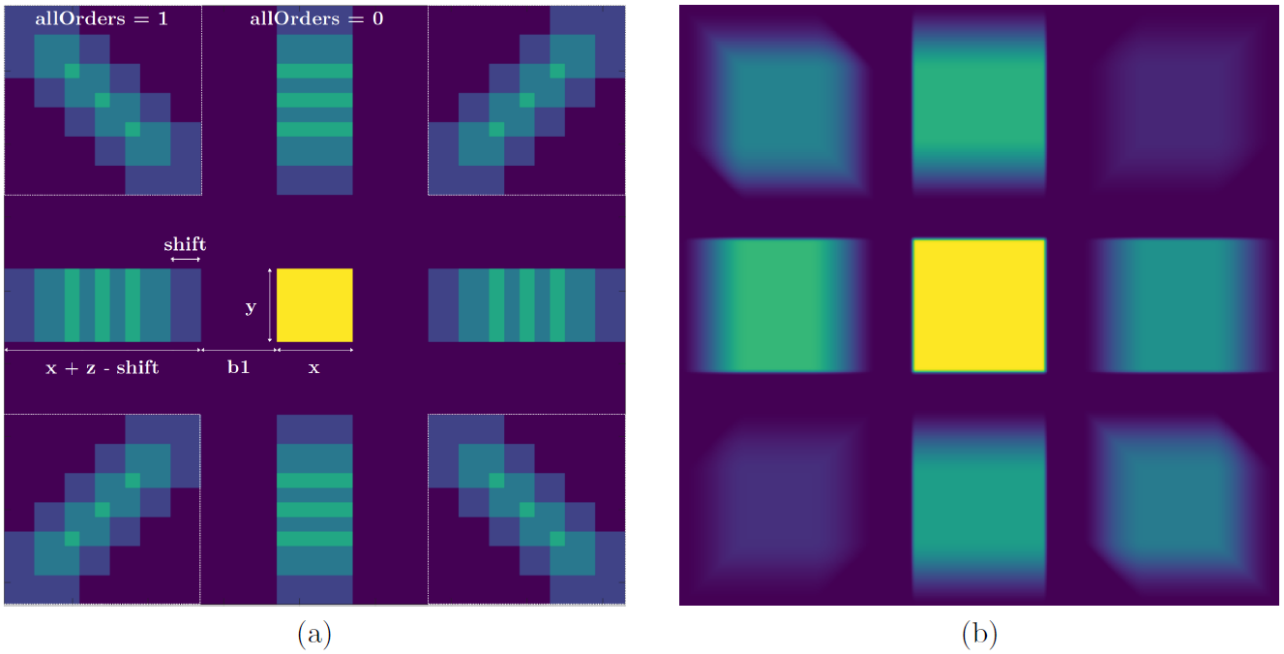

Figure S1: (a) Visual overview of the correspondence between the geometric inputs of the CTIS simulator and the simulated CTIS image for inputs x, y, z, $b1 = 5$, $b2 = 0$, $shift = 2$, $allOrders = True$, and without $sigma\_psf$, $diff\_sens$, $illum$ and $noise$. (b) Simulated CTIS image for $x, y = 100$, $z = 25$ $b1 = 27$, $b2 = 0$, $shift = 2$, $allOrders = True$, $sigma\_psf = 1.04$ and $noise = 0.44$. While $diff\_sens$ and $illum$ are set to the values defined in section S4

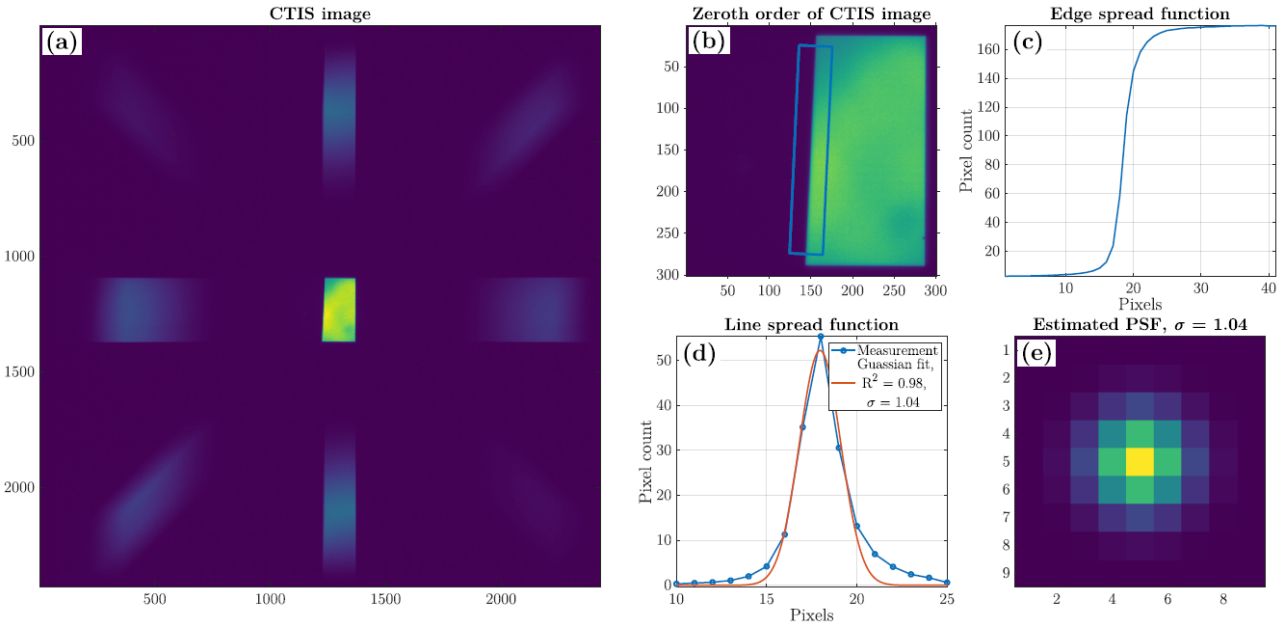

Figure S2: (a) CTIS image of a slanted razorblade back illuminated by tungsten halogen lamps for point spread function (PSF) estimation. (b) Zeroth order of CTIS image with 250×40 pixels blue rectangle used to estimate the (c) edge spread function (ESF) (mean across 250 pixels) and (d) line spread function (LSF) (derivative of ESF). The standard deviation of the LSF is estimated from a Gaussian fit, and (e) depicts the estimated symmetric PSF.

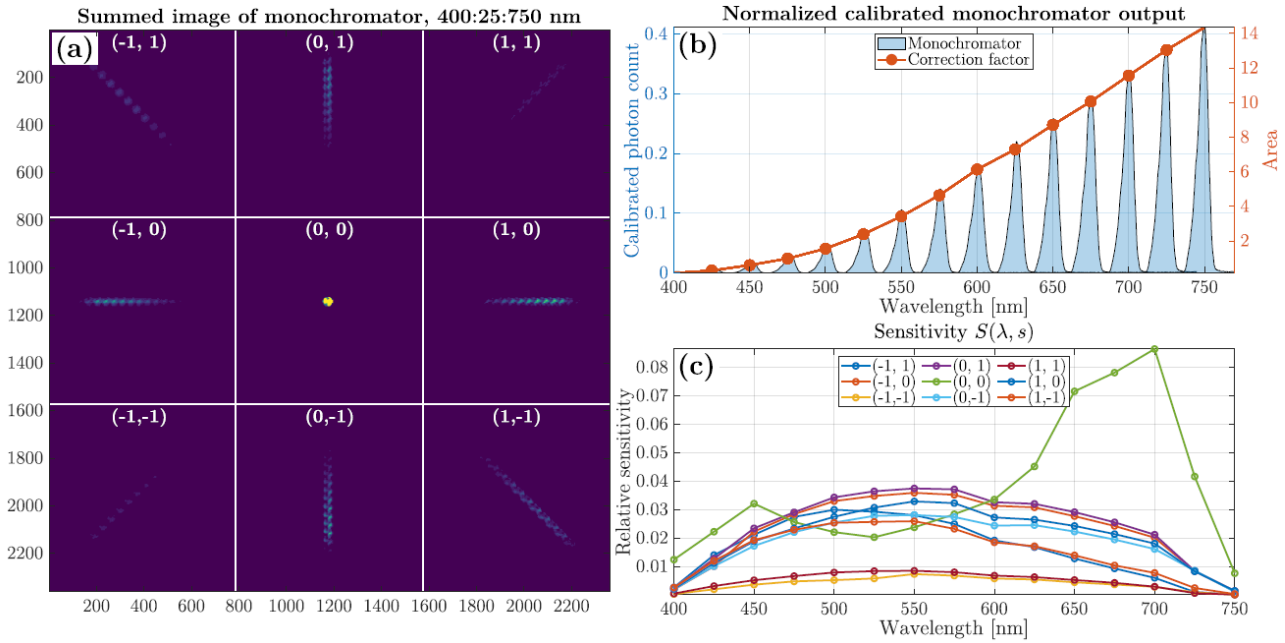

Figure S3: (a) Superimposed image consisting of monochromator images for 400-750 nm with 25 nm steps. (b) Normalized monochromator photon count measured with a calibrated Avaspec 2048x14 spectrometer, and correction factors corresponding to the area under the curve. (c) calculated diffraction sensitivity $S(\lambda, s)$ for the wavelength range 400-750 nm and the 9 diffraction spots.

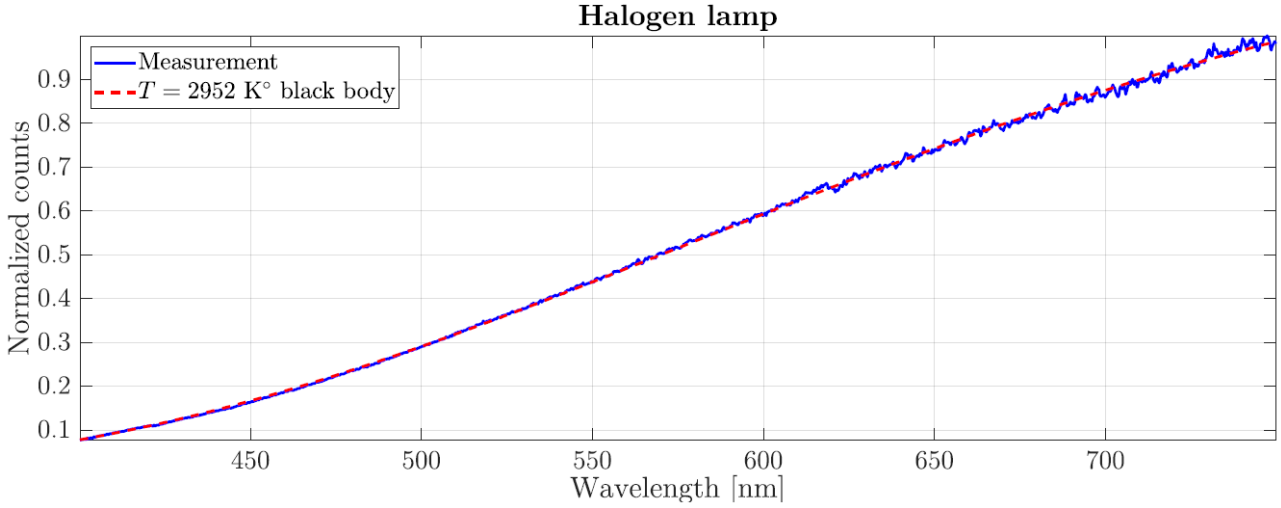

Figure S4: Measured spectrum of the industrial 3000 $K°$ halogen lamps used as illumination for CTIS images and a fitted black body with a temperature of $T = 2952\ K°$

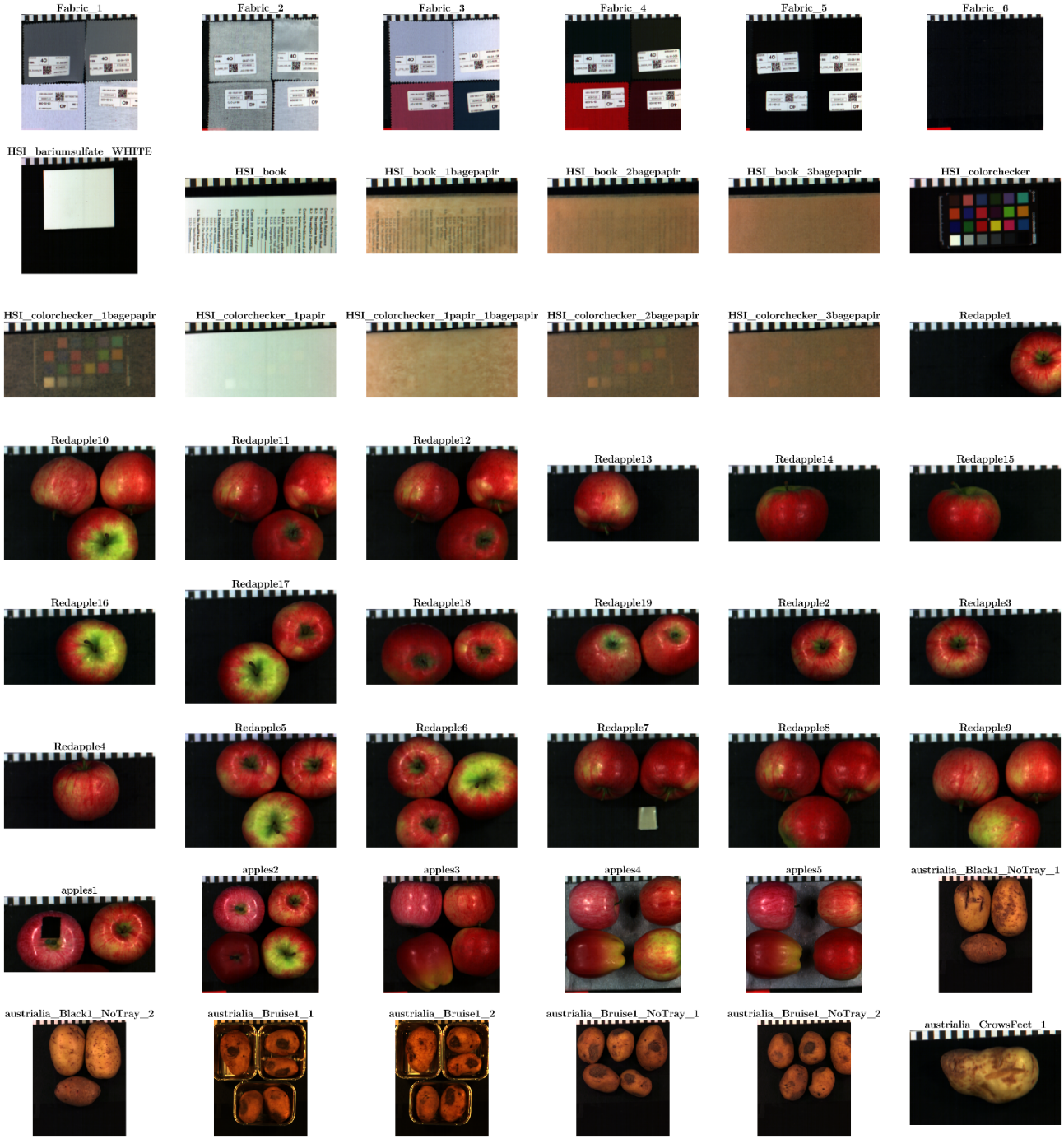

Figure S5: (1) RGB reconstructions of hyperspectral images captured with the pushbroom system and used in the training of the neural networks.

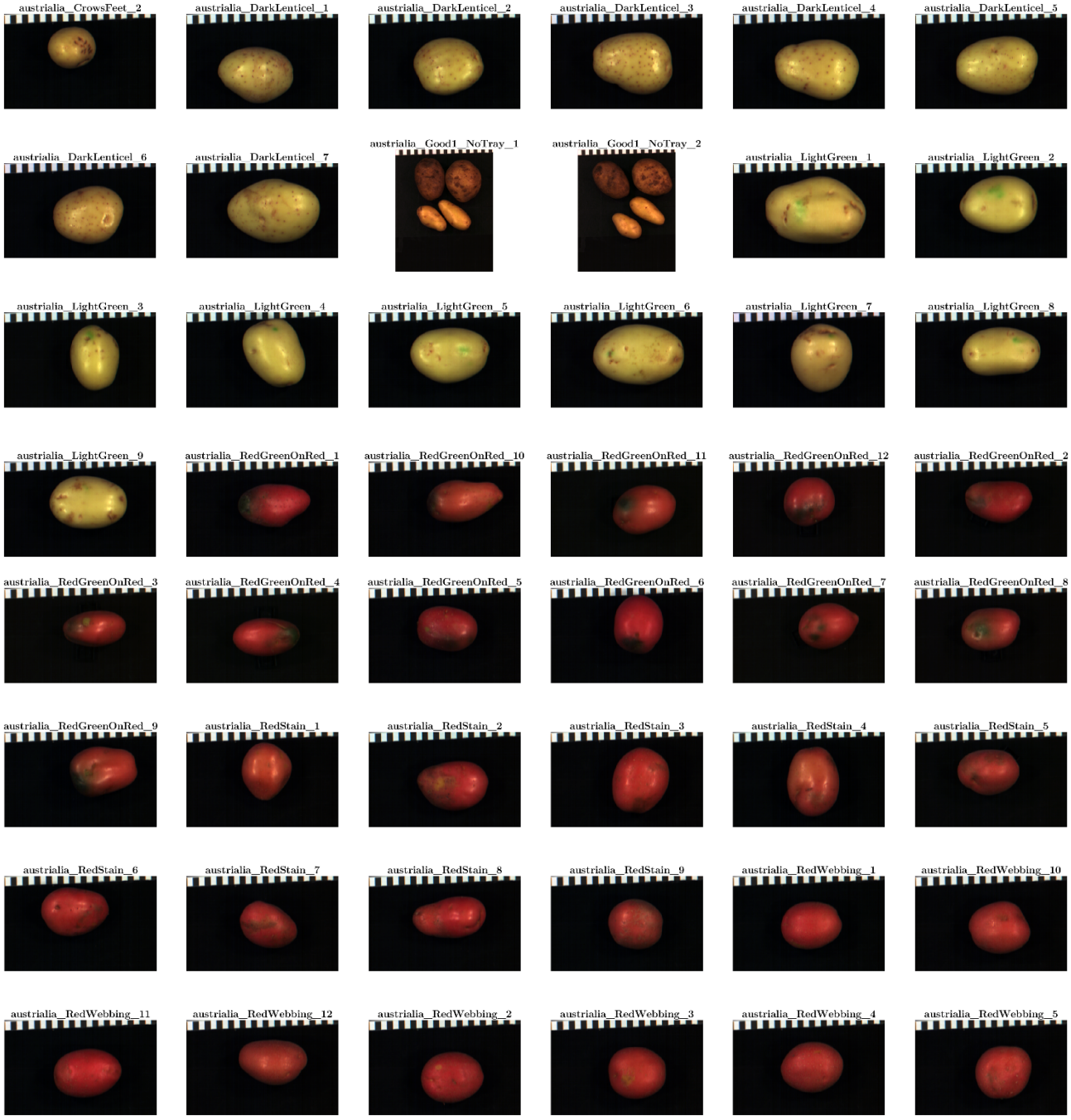

Figure S6: (2) RGB reconstructions of hyperspectral images captured with the pushbroom system and used in the training of the neural networks.

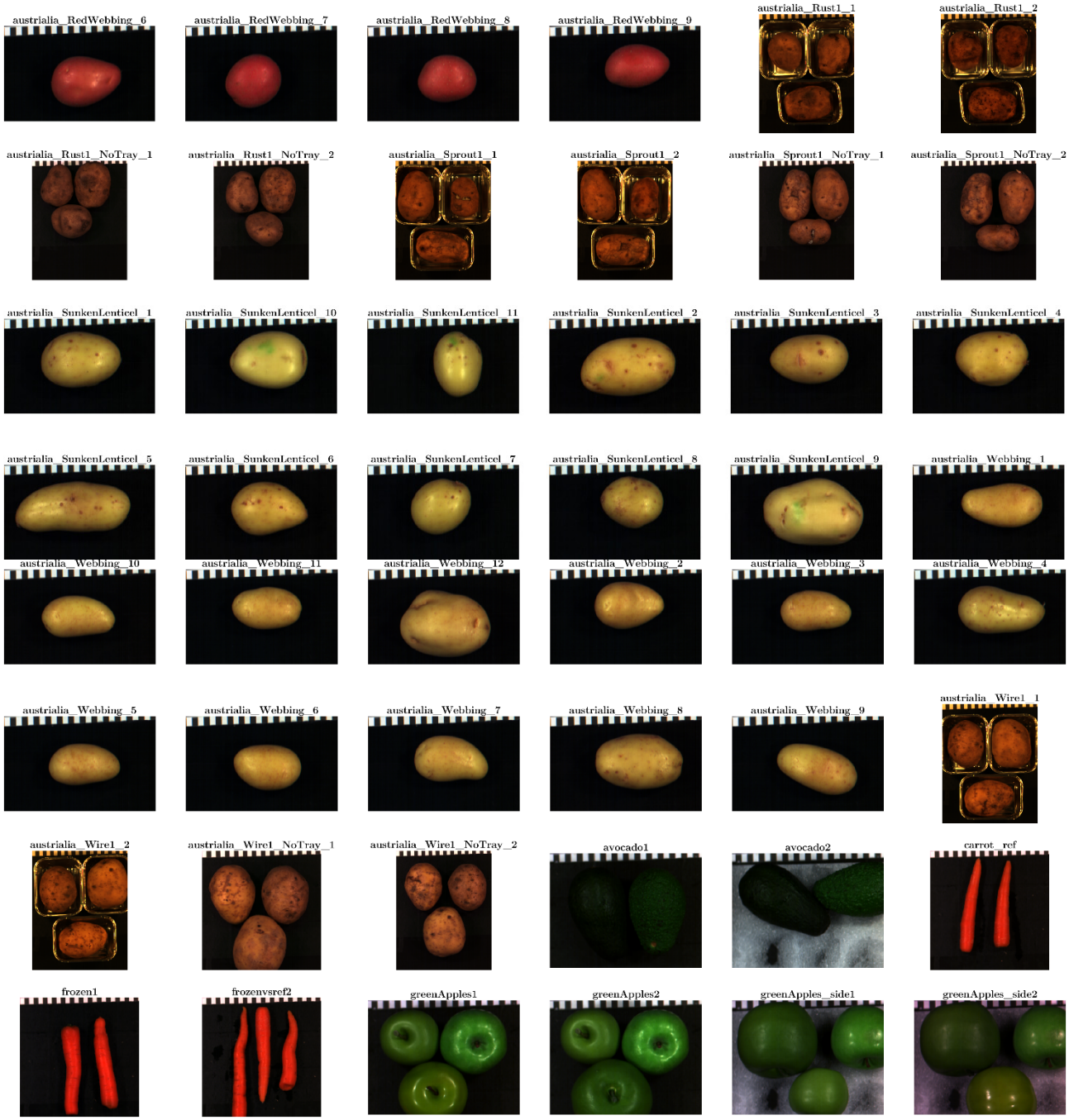

Figure S7: (3) RGB reconstructions of hyperspectral images captured with the pushbroom system and used in the training of the neural networks.

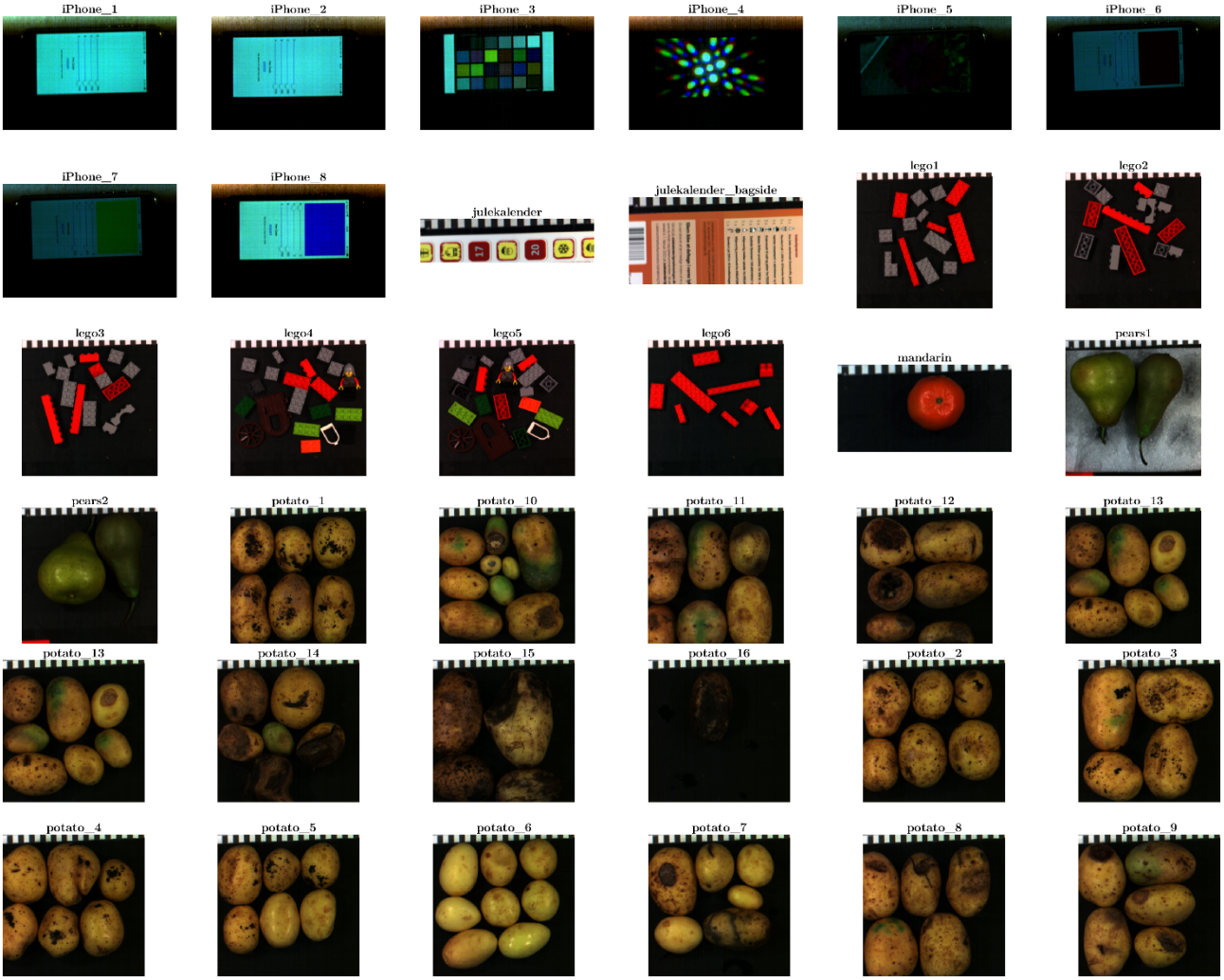

Figure S8: (4) RGB reconstructions of hyperspectral images captured with the pushbroom system and used in the training of the neural networks.

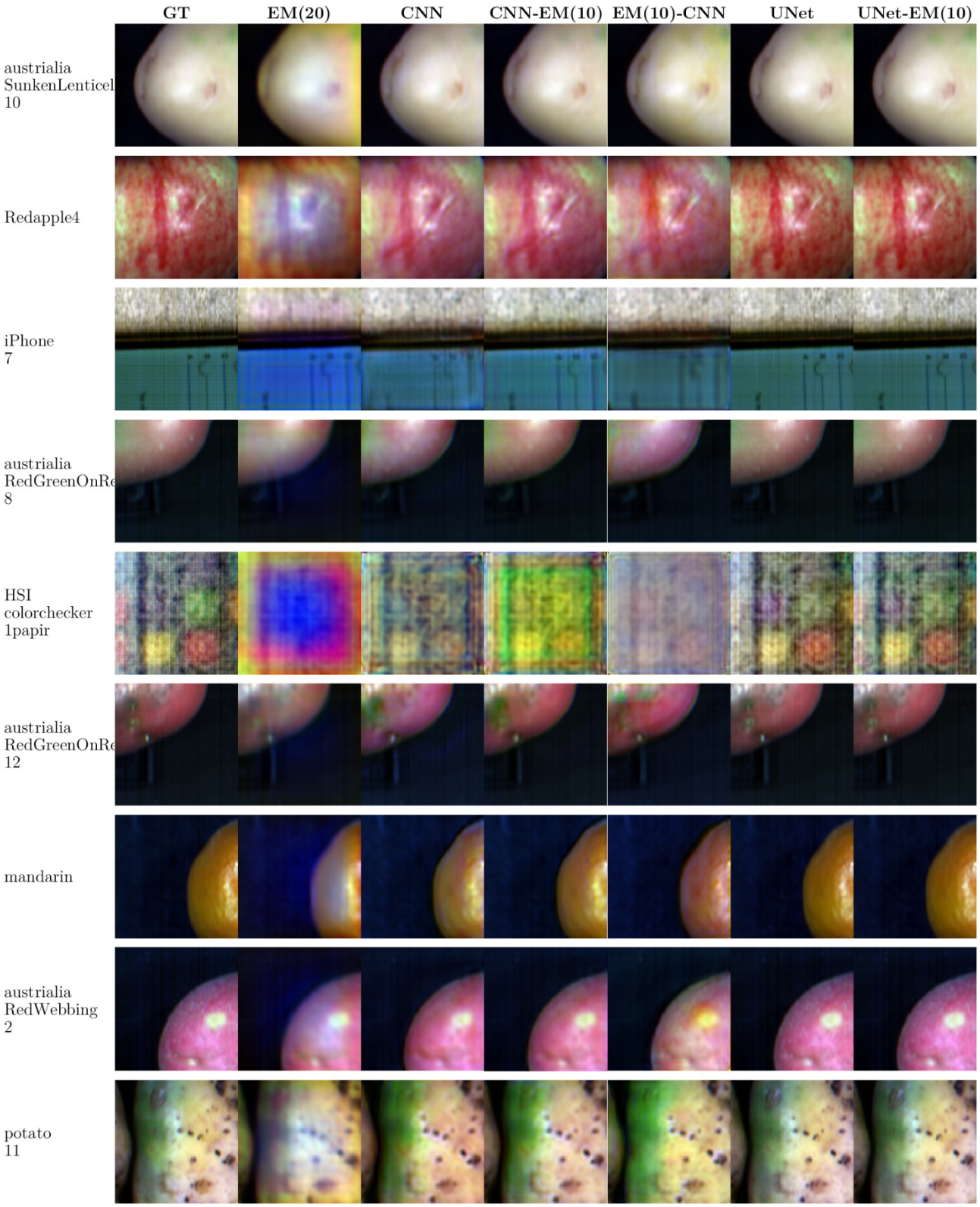

Figure S9: RGB comparison of reconstructed hyperspectral cubes (seen) for 25 channels. RGB images are generated from spectral channel 7, 9 and 13.

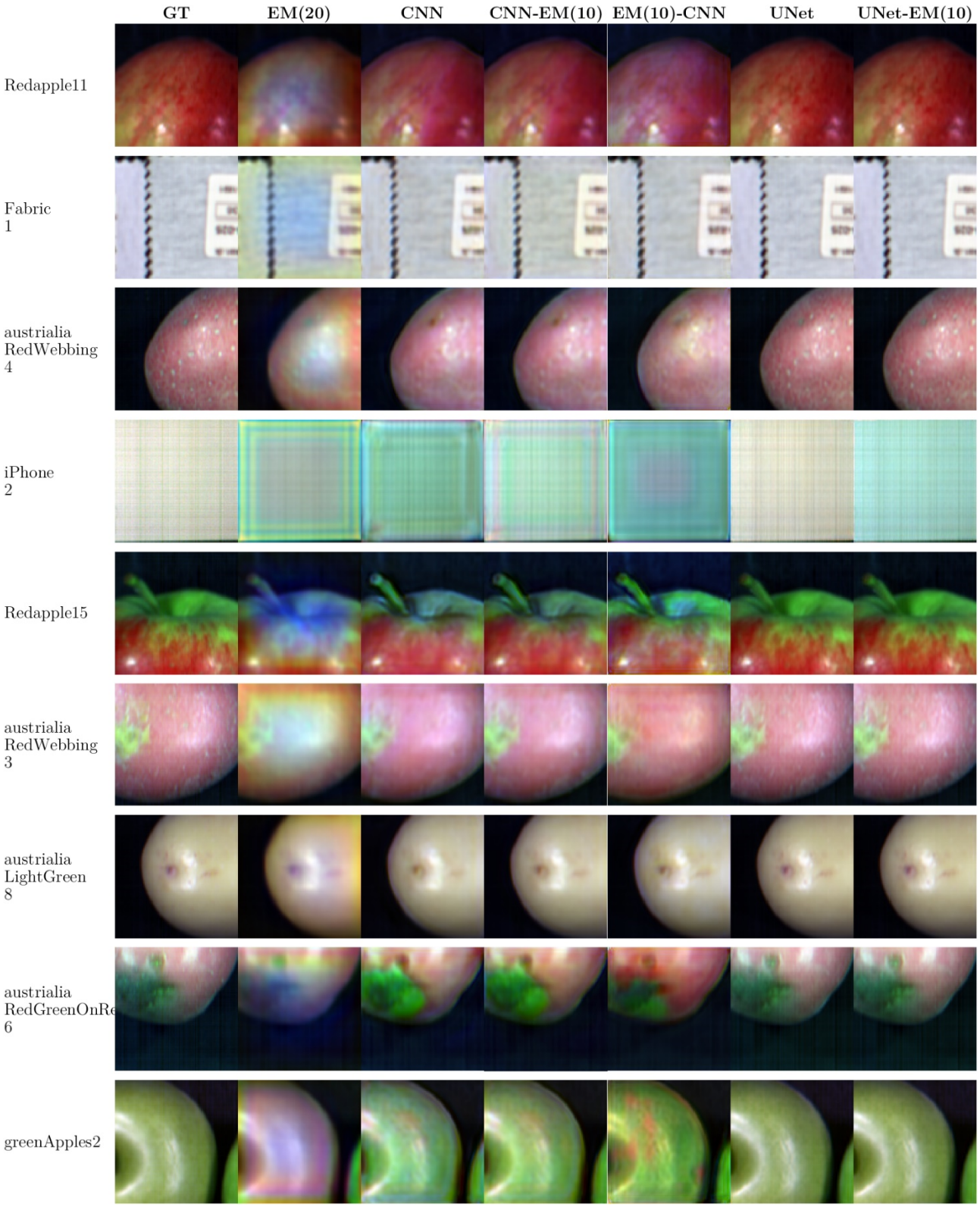

Figure S10: RGB comparison of reconstructed hyperspectral cubes (seen) for 25 channels. RGB images are generated from spectral channel 7, 9 and 13.

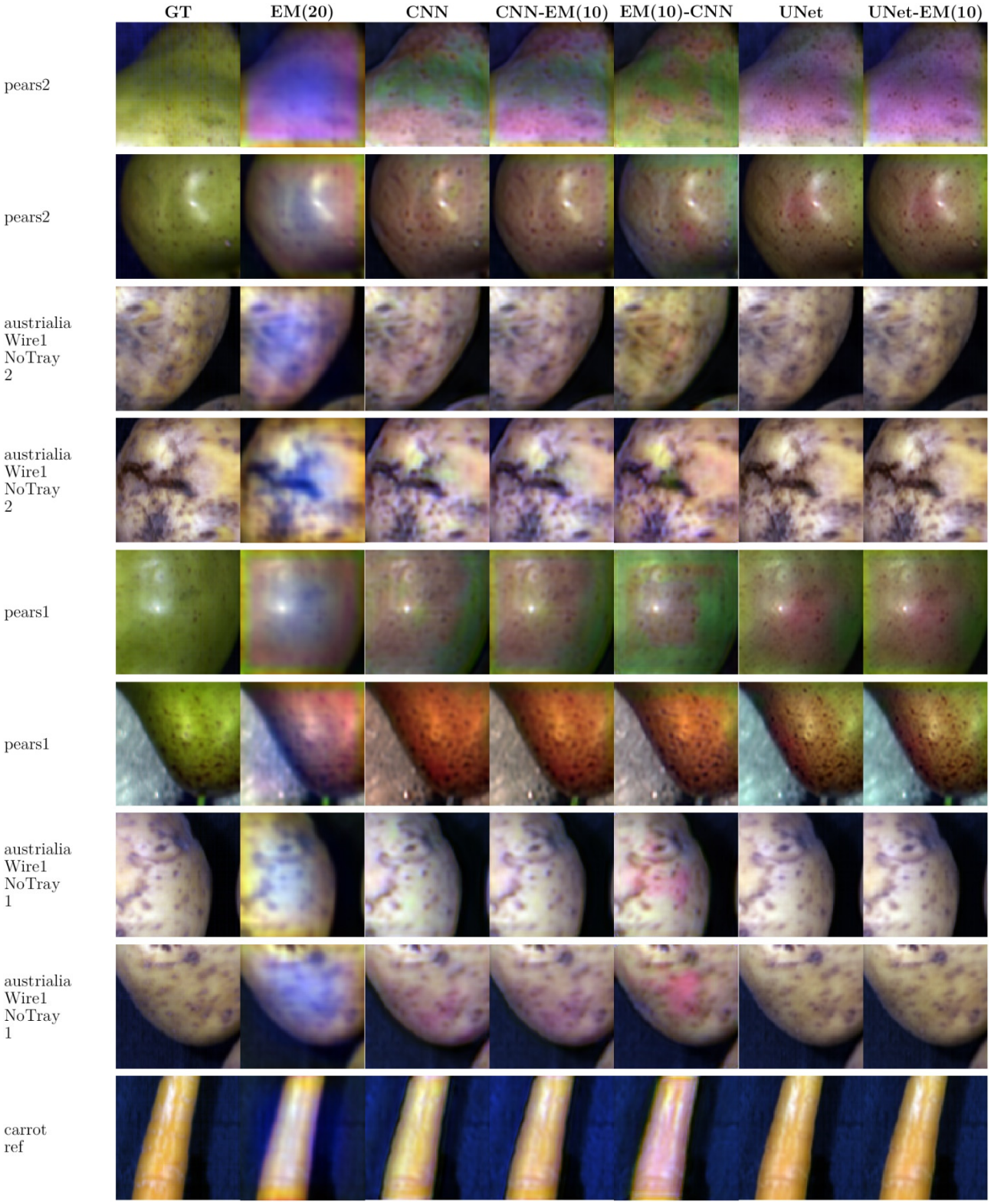

Figure S11: RGB comparison of reconstructed hyperspectral cubes (unseen) for 25 channels. RGB images are generated from spectral channel 7, 9 and 13.

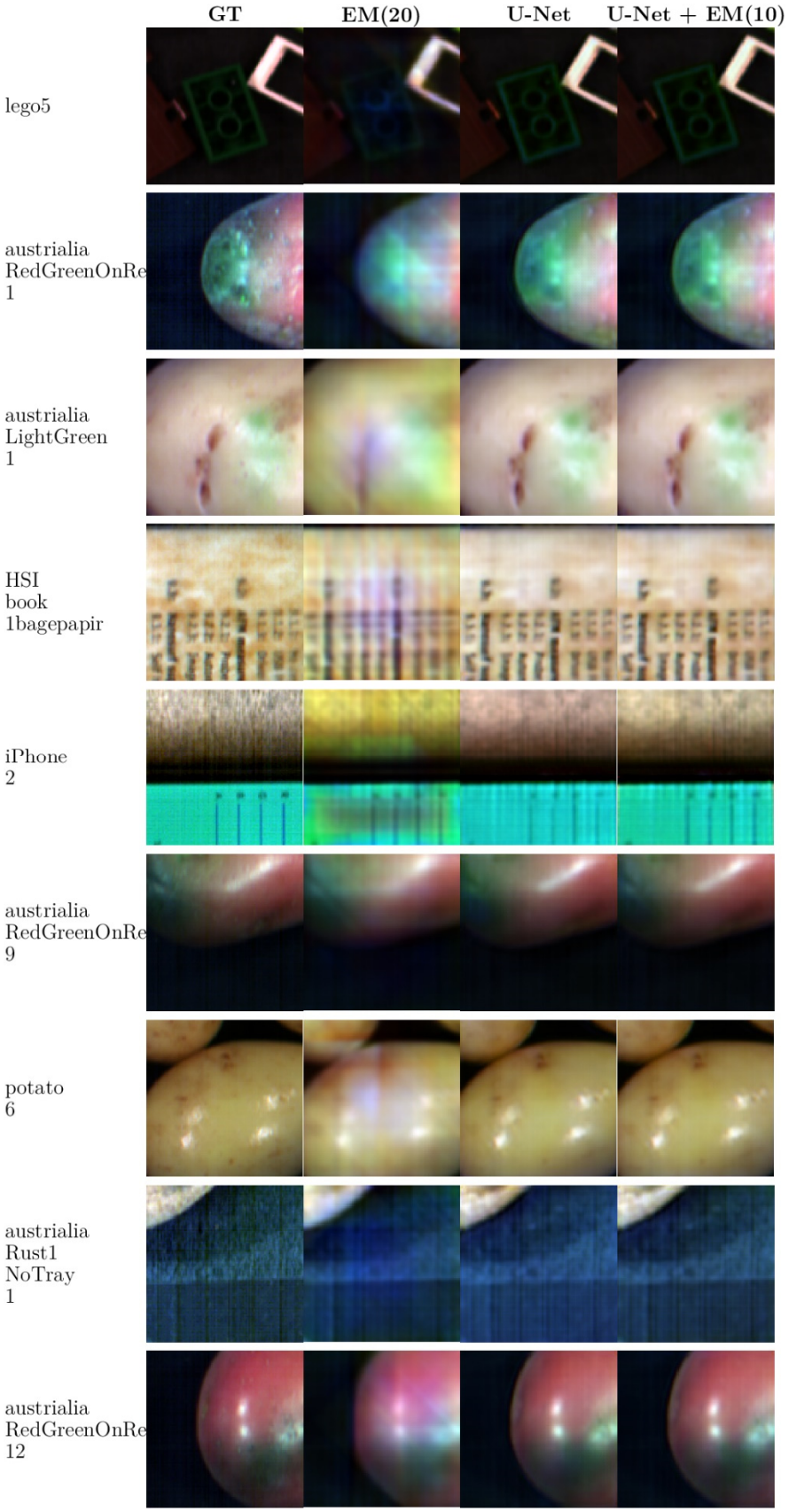

Figure S12: RGB comparison of reconstructed hyperspectral cube (seen) for 100 channels. RGB images are generated from spectral channel 14, 29 and 48

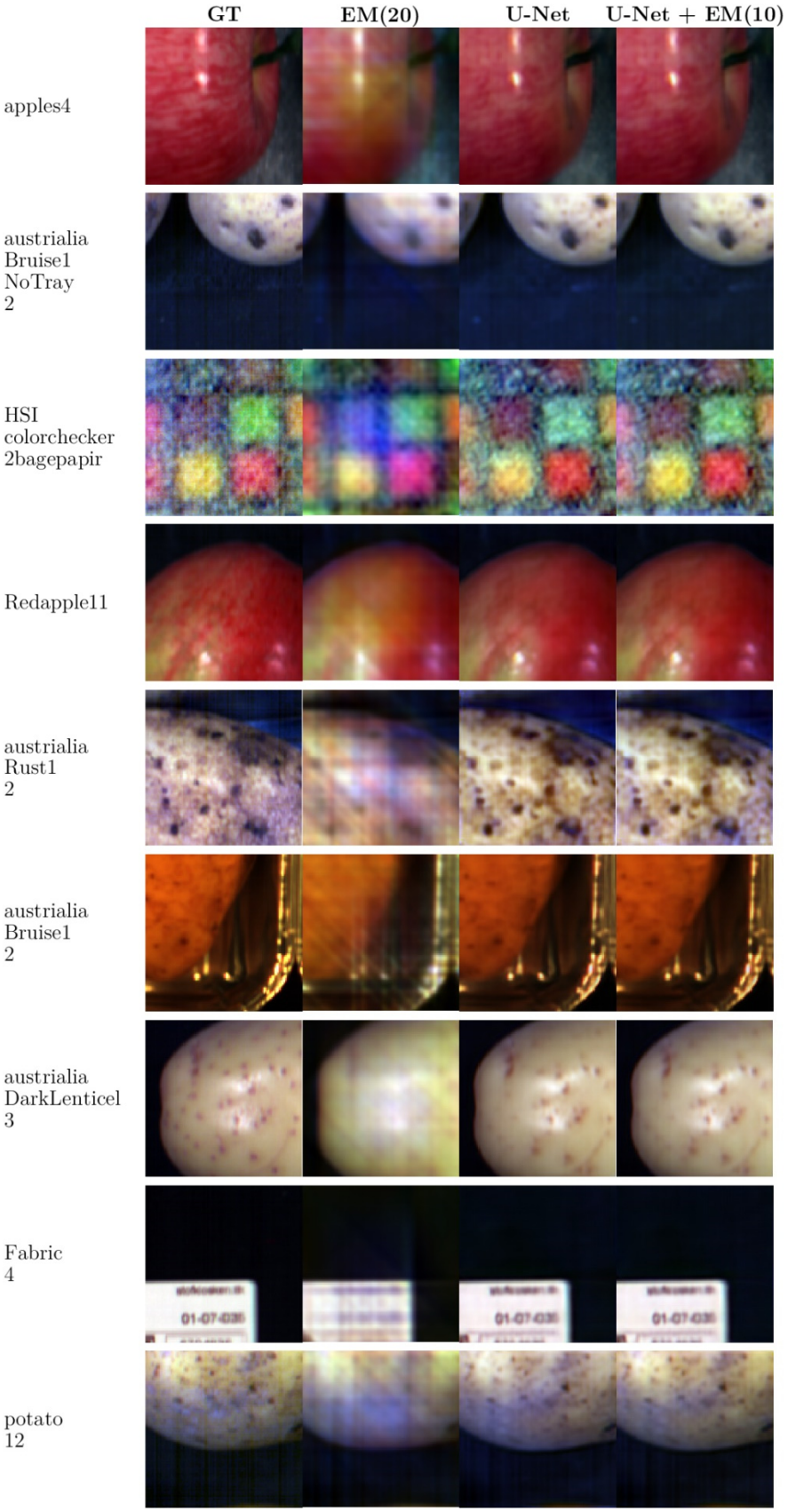

Figure S13: RGB comparison of reconstructed hyperspectral cube (seen) for 100 channels. RGB images are generated from spectral channel 14, 29 and 48

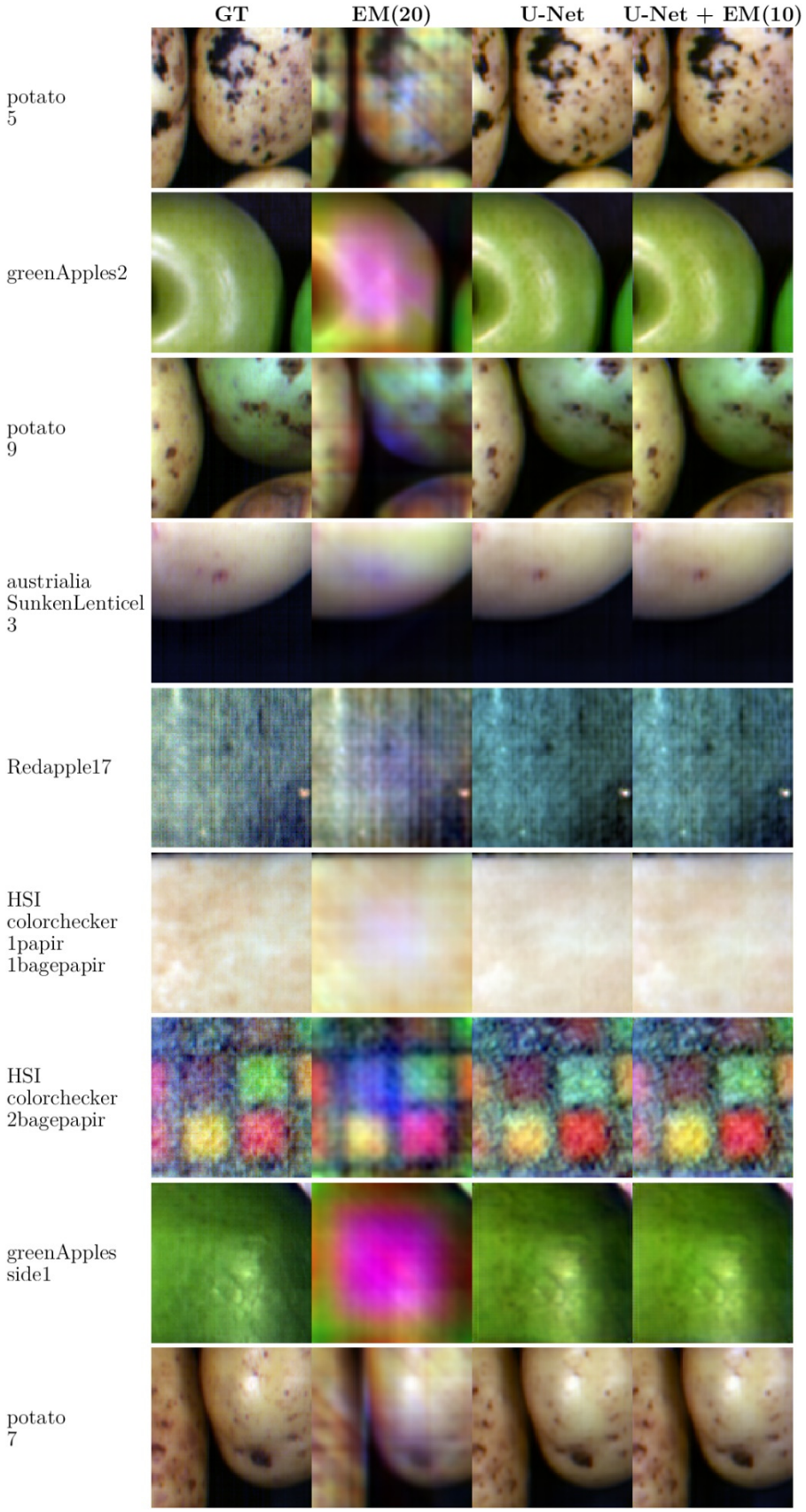

Figure S14: RGB comparison of reconstructed hyperspectral cube (unseen) for 100 channels. RGB images are generated from spectral channel 14, 29 and 48